

Accepted Manuscript

Diagnostic performance of a novel 3D neuroretinal rim parameter for glaucoma using high-density volume scans

Eric Shieh, Ramon Lee, Christian Que, Vivek Srinivasan, Rong Guo, Regina DeLuna, Sumir Pandit, Huseyin Simavli, Rajini Seevaratnam, Edem Tsikata, Johannes de Boer, Teresa Chen

PII: S0002-9394(16)30301-4

DOI: [10.1016/j.ajo.2016.06.028](https://doi.org/10.1016/j.ajo.2016.06.028)

Reference: AJOPHT 9791

To appear in: *American Journal of Ophthalmology*

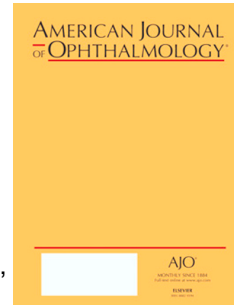
Received Date: 31 January 2016

Revised Date: 15 June 2016

Accepted Date: 16 June 2016

Please cite this article as: Shieh E, Lee R, Que C, Srinivasan V, Guo R, DeLuna R, Pandit S, Simavli H, Seevaratnam R, Tsikata E, de Boer J, Chen T, Diagnostic performance of a novel 3D neuroretinal rim parameter for glaucoma using high-density volume scans, *American Journal of Ophthalmology* (2016), doi: 10.1016/j.ajo.2016.06.028.

This is a PDF file of an unedited manuscript that has been accepted for publication. As a service to our customers we are providing this early version of the manuscript. The manuscript will undergo copyediting, typesetting, and review of the resulting proof before it is published in its final form. Please note that during the production process errors may be discovered which could affect the content, and all legal disclaimers that apply to the journal pertain.



Abstract

1

Purpose: To evaluate the diagnostic performance of a three-dimensional (3D) neuroretinal rim parameter, the minimum distance band (MDB), using optical coherence tomography high-density volume scans for open angle glaucoma.

Design: Reliability analysis.

Methods: Setting: Institutional. Study population: 163 patients (105 glaucoma and 58 healthy subjects). Observation procedures: One eye of each patient was included. MDB and retinal nerve fiber layer (RNFL) thickness values were determined for 4 quadrants and 4 sectors using the Spectralis SD-OCT device. Main outcome measures: Area under the receiver operating characteristic curve (AUROC) values, sensitivities, specificities, and positive and negative predictive values.

Results: The best AUROC values of 3D MDB thickness for glaucoma and early glaucoma were for the overall globe (0.969, 0.952), followed by the inferior quadrant (0.966, 0.949) and inferior-temporal sector (0.966, 0.944), and then followed by the superior-temporal sector (0.964, 0.932) and superior quadrant (0.962, 0.924). All 3D MDB thickness AUROC values were higher than those of 2D RNFL thickness. Pairwise comparisons showed that the diagnostic performance of the 3D MDB parameter was significantly better than 2D RNFL thickness only for the nasal quadrant and inferior-nasal and superior-nasal sectors ($p = 0.023-0.049$). Combining 3D MDB with 2D RNFL parameters provided significantly better diagnostic performance (AUROC 0.984) than most single MDB parameters and all single RNFL parameters.

Conclusions: Compared to the 2D RNFL thickness parameter, the 3D MDB neuroretinal rim thickness parameter had uniformly equal or better diagnostic performance for glaucoma in all regions and was significantly better in the nasal region.

Diagnostic performance of a novel 3D neuroretinal rim parameter for glaucoma using high-density volume scans 1

Eric Shieh,¹ Ramon Lee,¹ Christian Que,^{1,2} Vivek Srinivasan,^{1,2} Rong Guo,³ Regina DeLuna,⁴ Sumir Pandit,¹ Huseyin Simavli,^{1,2} Rajini Seevaratnam,⁵ Edem Tsikata,^{1,2} Johannes de Boer,⁶ Teresa Chen^{1,2}

¹Harvard Medical School, Boston, MA

²Department of Ophthalmology, Massachusetts Eye and Ear Infirmary, Boston, MA

³Biostatistics, Massachusetts Eye and Ear Infirmary, Boston, MA

⁴Johns Hopkins University School of Medicine, Baltimore, MD

⁵New England College of Optometry, Boston, MA

⁶Department of Physics and Astronomy, Vrije Universiteit, Amsterdam, Netherlands

Correspondence:

Teresa C. Chen, MD
Massachusetts Eye and Ear Infirmary, Glaucoma Service
243 Charles Street,
Boston, MA 02114
Tel: 617-573-6460
Fax: 617-573-3707
teresa_chen@meei.harvard.edu

Short title: Neuroretinal rim measurement in glaucoma using 3D scans

Key words: Neuroretinal rim, optic nerve head, optical coherence tomography, glaucoma

Introduction

2

Glaucoma is characterized by the loss of retinal ganglion cells and their axons, resulting in structural changes of the optic nerve head (ONH) and functional visual field (VF) loss. The diagnosis of glaucoma relies on structural and functional assessments, which have traditionally included disc photography and visual field testing. While informative, these methods rely on subjective interpretations, have high inter-rater variability, and provide little quantitative data.¹

The introduction of new imaging modalities, such as spectral domain optical coherence tomography (SD-OCT), have enabled more objective, reliable, and quantitative assessments of glaucoma.² Measurements of the ONH, peripapillary nerve fiber layer (RNFL), and macular ganglion cell region are useful structural surrogates for glaucomatous nerve loss.³⁻⁹ Of these parameters, the two-dimensional (2D) RNFL thickness measurement is the most widely used clinically.^{5,10-13} Despite its good-to-excellent diagnostic performance, RNFL thickness measurements have limitations, including a high frequency of SD-OCT-related imaging artifacts.¹⁴⁻¹⁷ Furthermore, RNFL thickness testing has high false positive rates of up to 26.2% to 39%, especially in patients with longer axial lengths and smaller disc areas.^{18,19}

Because of the limitations of current 2D glaucoma imaging parameters, novel three-dimensional (3D) neuroretinal rim parameters have been described^{20,21} and include the minimum distance band (MDB) which is derived from high-density volume scans.^{20,21} The MDB is the 3D region delimited by the shortest distances between the internal limiting membrane (ILM) and the optic disc margin, which is presumed to be the retinal pigment epithelium/Bruch's membrane (RPE/BM) complex termination. MDB thinning may be a proxy for nerve loss, since all retinal ganglion axons pass through the MDB to reach the brain and since more than 90% of the tissue in the MDB region is estimated to consist of ganglion cell nerve axons.²²

The 3D MDB thickness parameter has several advantages over other SD-OCT neuroretinal rim parameters. One advantage is that the MDB is measured perpendicular to the trajectory of nerve axons, factoring for the rim tissue's variable orientation.^{20,21,23-26} Second, MDB thickness defines the OCT-derived optic disc margin using the RPE/BM complex termination, an objective and easily identifiable anatomic landmark in OCT. By contrast, traditional neuroretinal rim parameters (e.g., cup-to-disc ratio, rim area) define the optic disc margin as the clinical optic disc margin, which is based on a subjective evaluation of the ONH. Reis *et al.* have shown that the clinical optic disc margin corresponds poorly with a single consistent anatomic structure in SD-OCT, such that "current rim measurements lack a solid anatomical foundation."^{23-25,27-29}

Current optic nerve parameters are derived from low-density scan protocols, and to date, no published studies have evaluated the diagnostic accuracy of the MDB thickness parameter using high-density 3D volume scans.^{30,31} Since volume scans enable denser sampling of nerve tissue and 3D reconstruction of neuroretinal rim anatomy compared to conventional 2D scans, we hypothesized that 3D volume scans

would have improved diagnostic performance for glaucoma. The aims of this study³ were to evaluate the diagnostic performance of the 3D MDB thickness parameter using high-density volume scans and to compare the diagnostic performance of MDB thickness with that of 2D RNFL thickness. We also assessed the diagnostic performance of combinations of MDB and RNFL parameters compared to single MDB and RNFL parameters alone.

Methods

4

Participants and examinations: The study was approved by the Massachusetts Eye and Ear Infirmary Institutional Review Board. Informed consent was obtained, and all methods adhered to the Health Insurance Portability and Accountability Act. Study participants were recruited from the Massachusetts Eye and Ear Infirmary Glaucoma Service between September 2009 and July 2014. Complete eye examinations were performed by one glaucoma specialist (T.C.C.) and consisted of history, visual acuity testing, refraction, Goldmann applanation tonometry, slit-lamp biomicroscopy, gonioscopy, ultrasonic pachymetry, dilated ophthalmoscopy, stereo disc photography (Visucam Pro NM; Carl Zeiss Meditec, Inc.), VF testing (Swedish Interactive Threshold Algorithm 24-2 test of the Humphrey visual field analyzer 750i; Carl Zeiss Meditec, Inc.), and volume scans using Spectralis OCT (HRA/Spectralis software version 5.4.8.0, Heidelberg Engineering GmbH, Heidelberg, Germany).

The study population consisted of participants with and without glaucoma with a spherical equivalent between -5.0 and +5.0 diopters and reliable VF test results with $\leq 33\%$ fixation losses, $\leq 20\%$ false-positive results, and $\leq 20\%$ false-negative results. Exclusion criteria were discernible congenital anomalies of the anterior chamber, corneal scarring or opacities, severe non-proliferative or proliferative diabetic retinopathy, any disease that could independently affect VF, VF loss due to a non-glaucoma condition (e.g., trauma), or a dilated pupil diameter of less than 2 mm.

Open angle glaucoma was defined as characteristic optic nerve changes with corresponding VF defects. A VF was abnormal if 3 or more contiguous test locations in the pattern deviation plot were depressed by ≥ 5 decibels (dB). Glaucoma was also diagnosed if 2 or more contiguous test locations had defects with one location depressed by ≥ 5 dB and the other by ≥ 10 dB. Test locations on the pattern deviation plot's outer rim were excluded to avoid rim artifacts. Patients with primary open angle, normal tension, pseudoexfoliation, and pigmentary glaucoma with best-corrected visual acuities of 20/70 or better were included. VF abnormalities were classified as early (mean deviation [MD] > -6 dB), moderate (-12 dB $< MD \leq -6$ dB), or severe ($MD \leq -12$ dB).

Normal subjects had no ocular disease except for mild cataracts, normal VF test results defined by a pattern standard deviation (PSD) of more than 5%, normal glaucoma hemifield test results, best-corrected visual acuities of 20/40 or better, and no cup to disc asymmetry of greater than 0.2 between eyes. If both eyes were eligible, one eye was selected using a random number generator. Investigators were masked to the OCT results at the time of participant selection.

Image acquisition and automated segmentation: After pupillary dilation, each eye underwent peripapillary RNFL thickness scans and 20 x 20 degree volume scans centered on the ONH using the Spectralis SD-OCT machine. For volume scans, 193 frames were taken with the high-speed rate. Three averages were acquired per frame with the automatic real-time function activated, enabling the acquisition of multiple

frames at the same scan location and the averaging of the frames to reduce noise and 5 eye motion artifacts. Scans meeting the following criteria were included for analysis: signal strengths of 15 dB or more (range: 0 to 40 dB), clear fundus images with good optic disc and scan circle visibility before and during image acquisition, visible RNFLs without interruptions, and continuous scan patterns without missing or blank areas. Details of the Spectralis SD-OCT technique have been described elsewhere.^{32,33}

2D RNFL thickness values were extracted from Spectralis SD-OCT RNFL printouts and calculated globally and sectorally as means. 3D volumetric data was downloaded as series of images in PNG format. The program to determine the MDB was coded in C++ using the Open Computer Vision (OpenCV), Insight Segmentation and Registration Toolkit (ITK, Insight Software Consortium), and Visualization Toolkit (VTK, Kitware Inc., Clifton Park, New York) libraries (E.T.). The optic disc margin, presumed to be the termination of the RPE/BM complex, was represented by 100 points spaced by 3.6 degrees. Segmented images were manually reviewed. Frames with acquisition artifacts or algorithm errors were discarded. The accuracy of the optic disc rim in OCT images was verified by superimposing the points on an infrared reflectance (IR) image of the ONH. The reconstructed ILM and RPE/BM complex were manually inspected in 3D for errors. Eyes were excluded when the RPE/BM complex was incompletely identified due to noisy data or prominent blood vessels, leading to more than five consecutive errors over the ONH. The optic disc center was automatically determined from IR fundus photos and OCT scans. Images were automatically segmented with an internally developed program to delineate the RPE/BM complex and the ILM (**Figure 1**). An internal algorithm calculated MDB thickness values using the distances between points along the RPE/BM complex termination and the closest corresponding points on the ILM. MDB thickness values were calculated for the overall globe (360 degrees), 90 degree quadrants (inferior, superior, nasal, and temporal), and 45 degree sectors (inferior-nasal [IN], superior-nasal [SN], inferior-temporal [IT], and superior-temporal [ST]).

Statistical analysis: Statistical analyses were performed with SAS 9.4 (SAS Institute Inc., Cary, NC). Descriptive characteristics were reported as mean +/- standard deviation for continuous variables and frequency count (%) for categorical variables. Student's t-tests were used to compare continuous variables, and Chi-square tests for categorical variables. P-values of < 0.05 established statistical significance.

The diagnostic performances of 2D RNFL and 3D MDB parameters were determined using receiver operating characteristic (ROC) curves and calculating areas under the ROC curves (AUROC). An optimal cut-off value was selected using the Youden index value that maximized the value of "sensitivity + specificity - 1." Sensitivity, specificity, positive predictive values (PPV), and negative predictive values (NPV) were calculated using these cutoff values. Pairwise comparisons of AUROC values were performed to compare accuracy between measurements. Diagnostic test performance was classified as excellent for AUROC values of 0.90-1.00, good (0.80-0.90), fair (0.70-0.80), and poor (0.60-0.70).

Stepwise logistic regression was used to identify the best combinations of MDB and RNFL parameters for glaucoma diagnosis. The combinations of MDB parameters, RNFL parameters, and MDB and RNFL parameters that yielded the highest AUROC values were determined. The AUROC of the best combination of MDB and RNFL parameters was compared with that of the best combinations of MDB parameters and RNFL parameters. 6

Results

7

The study consisted of 163 participants, of which 105 were glaucoma patients and 58 were healthy controls (**Table 1**). Of the glaucoma patients, 70 of 105 (66.7%) patients had primary open angle glaucoma, 13 of 105 (12.4%) had normal tension glaucoma, 14 of 105 (13.3%) had pseudoexfoliation glaucoma, and 8 of 105 (7.6%) had pigmentary glaucoma. Severity of VF defects was distributed with 31 of 105 (29.5%) having early VF defects, 31 of 105 (29.5%) having moderate VF defects, and 43 of 105 (41.0%) having severe VF defects. The glaucoma group and early glaucoma group were significantly older ($p < 0.0001$) and had a smaller proportion of females ($p = 0.004$, $p = 0.029$) than the control group (**Table 1**). Compared to the control group, the glaucoma group and the early glaucoma group had significantly thinner MDB values in all quadrants and sectors ($p < 0.0001$; **Table 2**).

The MDB's diagnostic capability was evaluated by calculating AUROC values for glaucoma and early glaucoma patients (**Table 3**). For glaucoma, the best diagnostic performances for the MDB were for the overall globe (AUROC 0.969; 95% confidence interval [CI] 0.945-0.993), followed by the inferior quadrant (0.966; 95% CI 0.937-0.995) and inferior-temporal sector (0.966; 95% CI 0.939-0.994), and then followed by the superior-temporal sector (0.964; 95% CI 0.939-0.998) and superior quadrant (0.962; 95% CI 0.936-0.987). Diagnostic cut-off values for the three best MDB parameters, as determined by the Youden index, were 233.9 μm for the overall globe, 262.7 μm for the inferior quadrant, and 240.9 μm for the inferior-temporal sector. For these cutoffs, the respective sensitivities and specificities for the identification of glaucoma were 89.5% and 96.6% for the overall globe, 92.4% and 96.6% for the inferior quadrant, and 91.4% and 96.6% for the inferior-temporal sector (**Table 4**).

For early glaucoma, the highest-ranked AUROC values for the MDB were also for the overall globe (0.952; 95% CI 0.911-0.993), followed by the inferior quadrant (0.949; 95% CI 0.900-0.998) and inferior-temporal sector (0.944; 95% CI 0.888-1.000), and then followed by the superior-temporal sector (0.932; 95% CI 0.880-0.984) and superior quadrant (0.924; 95% CI 0.869-0.980; **Table 3**). Optimal early glaucoma diagnostic cut-off values were 270.1 μm for the overall globe, 262.3 μm for the inferior quadrant, and 236.2 μm for the inferior-temporal sector. For these cutoffs, the sensitivities and specificities for identification of early glaucoma were 96.8% and 84.5% for the overall globe, 87.1% and 96.6% for the inferior quadrant, and 83.9% and 96.6% for the inferior-temporal sector, respectively (**Table 5**).

To compare 3D MDB with 2D RNFL, we determined the diagnostic performance of the traditional RNFL thickness parameter for glaucoma (**Table 6**) and early glaucoma (**Table 7**). For both glaucoma and early glaucoma, the MDB parameters had AUROC values greater than those of the corresponding RNFL parameters (**Tables 3**). Even though all MDB AUROC values were higher than those of the RNFL thickness parameters, a pairwise comparison of MDB and corresponding RNFL parameters showed that, for glaucoma, the differences were only statistically significant in the nasal quadrant ($p = 0.023$), as well as the superior-nasal ($p = 0.023$) and inferior-nasal ($p =$

0.049) sectors. The AUROC values of other corresponding MDB and RNFL parameters differed non-significantly for glaucoma and early glaucoma (**Table 3**).

8

Stepwise logistic regression was used to determine the diagnostic performance of combinations of MDB and RNFL parameters for glaucoma (**Table 3**). The best combination of MDB and RNFL parameters, which was the and-logic combination of inferior MDB, superior-temporal MDB, superior-nasal MDB, and inferior RNFL, yielded a significantly higher AUROC value (0.984; 95% CI 0.966-1.000) than the best combination of RNFL parameters (0.966; 95% CI 0.939-0.993; $p = 0.018$). The best combination of MDB and RNFL parameters had a non-significantly higher AUROC value than the best combination of MDB parameters (0.981; 95% CI 0.963-0.999; $p = 0.319$). Compared to single RNFL and single MDB parameters, the combination of MDB with RNFL parameters had significantly better diagnostic performance for all comparisons ($p < 0.0001$ to $p = 0.031$) except for comparisons with global MDB ($p = 0.065$) and inferior MDB ($p = 0.061$).

Discussion

9

Our study shows that the MDB neuroretinal rim measurement derived from high-density 3D volume scans has excellent accuracy in distinguishing glaucomatous from healthy eyes, since MDB thickness is thinner in glaucomatous eyes (**Table 2**). Based on best AUROC and diagnostic values, optimal MDB parameters for glaucoma and early glaucoma were for the overall globe, followed by the inferior quadrant and inferior-temporal sector, followed by the superior-temporal sector and superior quadrant (**Table 3**). This pattern is consistent with known glaucoma pathophysiology, in which the inferior and superior poles are most susceptible to nerve loss. That the temporal sectors of the superior and inferior quadrants are the more sensitive regions for detecting glaucoma is in agreement with studies using 2D SD-OCT.^{5,7}

Compared to 2D RNFL thickness, MDB thickness from high-density 3D volume scans had uniformly equal or better diagnostic performances for glaucoma for all tested regions (**Table 3**). The neuroretinal rim MDB thickness measurement was only significantly better in the nasal quadrant and inferior-nasal and superior-nasal sectors ($p = 0.023-0.049$). Although the nasal RNFL region traditionally has had little diagnostic value in glaucoma patients since glaucoma preferentially causes superior and inferior RNFL thinning, this finding suggests that the nasal neuroretinal rim should not be ignored in clinical assessments using OCT. The 3D nasal neuroretinal rim may be more important in OCT assessments than the 2D nasal RNFL region, since the nasal neuroretinal rim in 3D volume scans may have fewer segmentation errors due to blood vessels artifacts. Also, the nasal neuroretinal rim normally has higher baseline thickness values (Table 2, mean normal value 312.4 ± 49.5 microns) compared to RNFL baseline thickness values (mean normal value 71.0 ± 13.8 microns), and detecting change using a 7 micron resolution technology is theoretically easier if the structure being measured is thicker.

It is unclear why 3D MDB parameters had universally equal or better diagnostic performances for glaucoma than 2D RNFL parameters. One possibility is that compared to RNFL thickness, MDB thickness is measured closer to the ONH, where changes in retinal topology may be more pronounced or manifest earlier in the disease process, as proposed by Chauhan *et al.*²⁹ Another explanation is that the MDB defines the OCT-derived disc margin as the RPE/BM complex termination, which has not been described in the literature to undergo a glaucoma-related loss of reflectivity. By contrast, RNFL thickness becomes more difficult to measure accurately with worsening glaucoma, which causes the RNFL to thin and lose reflectivity.^{2,34,35}

Other investigators have studied a parameter similar to MDB thickness called the Bruch's membrane opening-minimum rim width (BMO-MRW). BMO-MRW is the shortest distance between the Bruch's membrane opening (BMO) and the ILM.^{23,29} A key difference between MDB thickness and BMO-MRW is how the OCT-derived disc margin is defined. The OCT disc margin is defined as the RPE/BM complex termination for MDB thickness measurements and as the BMO for BMO-MRW measurements.²¹ On histology, Bruch's membrane is only 1-5 μm in thickness, smaller than the resolution of

most commercially available SD-OCT instruments. Ultra high resolution OCT, used 10 mostly in the research setting, can have axial resolutions of 2-3 μm , while commercially available SD-OCT machines, including the Spectralis machine, have axial resolutions of 5-7 μm . While the Bruch's membrane may be visible in SD-OCT as a distinct structure in very rare cases, it is usually indistinguishable from the RPE, as noted by a consensus group of international SD-OCT experts, by several research groups, and by the current study, in which we could not resolve the Bruch's membrane in isolation for any of the study participants.^{27,36-38} We suggest that the RPE/BM complex termination is a better OCT-derived disc margin than BMO, because it is more consistently visible in SD-OCT images, is more easily segmented, and is a stable imaging landmark.

The OCT-derived disc margin, however, can be affected by peripapillary atrophy, which is common in glaucoma, older age, and myopia.³⁹ In our study population, the incidence of peripapillary atrophy was 90/163 (or 55.2% of subjects). Histologic studies have shown that peripapillary atrophy may result in a beta zone, or a region characterized by Bruch's membrane denuded of RPE cells.^{39,40} The beta zone likely reflects atrophy of RPE cells and is significantly larger in glaucomatous eyes than normal eyes.⁴⁰ This suggests that the BMO may more accurately reflect the disc border on histology; however, in actual OCT images, the RPE/BM complex is likely a more robust OCT-based disc margin as it is more consistently resolvable in SD-OCT images since the average BMO thickness is less than the axial resolution of commercially available SD-OCT machines. For example, in the current study where the RPE/BM complex was used as the OCT-derived disc border, we did not need to manually correct for segmentation errors of the RPE/BM complex in our patients with peripapillary atrophy, unlike the BMO-MRW parameter which may require manual correction of segmentation errors.²⁹ The RPE/BM complex likely represents a more robust OCT-derived disc margin, since this complex is more consistently visualized and is therefore easier to segment. Further studies are needed to evaluate the effect of various types of peripapillary atrophy on OCT-derived disc margin determinations.

Another difference between MDB thickness and BMO-MRW is that the 3D MDB thickness parameter is derived from high-density 3D volume scans with 193 raster lines. By contrast, the BMO-MRW is derived from lower density scans with 24 to 36 radial lines.^{26,29,41-44} It is unknown whether the high-density scan protocol used for the MDB measurement may yield higher AUROC values compared to the lower density scans for the BMO-MRW calculations. However, the high-density 3D volume scans have the advantage of allowing analysis of not only the 3D neuroretinal MDB parameter but also other 3D parameters such as cup volume, peripapillary RNFL volume, as well as peripapillary retinal volume.⁴⁵ Compared to MDB thickness, which had a best global AUROC value of 0.969, Chauhan *et al.* demonstrated a global BMO-MRW AUROC value of 0.96 using Spectralis, 24 radial scans, and manual segmentation of MDB boundaries.²⁹ Also using Spectralis and 24 radial scans, El Chehab *et al.* showed best BMO-MRW AUROC values of 0.890 for the overall globe and 0.881 for the inferior-temporal sector.⁴¹ In a third study using Cirrus software to automatically delineate MDB

boundaries from 36 radial scans, Pollet-Villard *et al.* achieved best BMO-MRW AUROC values of 0.906 for the overall globe and 0.917 for the inferior-temporal sector.²⁶

11

While the BMO-MRW has been shown to be better than RNFL thickness for glaucoma diagnosis, it is unclear whether the improvement is statistically significant as no p-values comparing AUROC curves were provided.³¹ Our results build on this finding and further show that the 3D MDB is significantly better than the 2D RNFL for the nasal quadrant ($p = 0.023$) and the inferior-nasal ($p = 0.049$) and superior-nasal sectors ($p = 0.023$; **Table 3**). We also found that the best combination of 3D MDB and 2D RNFL parameters for detecting glaucoma using the and-logic combination was also significantly better than all single 2D RNFL parameters alone ($p < 0.0001$ to $p = 0.018$). This finding is in line with prior studies showing that combining classic OCT parameters (i.e. RNFL, ONH, and macular ganglion cell complex) enhances diagnostic performance for glaucoma.^{6,46-48}

Measurement of the BMO-MRW has recently been incorporated into the Spectralis OCT Glaucoma Module Premium Edition.³³ Here, we detail the differences in spatial resolution, scan protocol, ONH centration, and segmentation technique between MDB thickness and BMO-MRW measurement using the Spectralis software. First, BMO-MRW uses keratometry for each patient to determine the spatial dimensions of the retina area under examination. Conversely, MDB thickness uses average conversion factors to convert from pixels to real-space dimension. Second, whereas BMO-MRW takes 24 radial cuts centered on the ONH and 25 averages per slice, MDB thickness uses 193 raster scans and 3 averages per slice. Third, BMO-MRW uses Anatomic Positioning System (APS) to determine the ONH center, which rotates the sectors of the retina according to each patient's fovea-to-Bruch's membrane opening center (FoBMOC) axis. Our group's approach to computing MDB thickness uses the calculated centroid of the optic disc. Finally, the two parameters utilize different segmentation techniques to delineate the OCT-derived outer margin. While BMO-MRW creates 48 points on the rim with BMO-MRW values evaluated from single points, MDB thickness utilizes 100 points on the rim, with each point being the closest point on the RPE/BM complex from the optic disc center in a 3.6 degree sector of the RPE/BM complex.

The current study has several limitations. For one, glaucoma patients were older than healthy subjects by an average of 14 years. Some studies have suggested an age-related loss of retinal ganglion cells with an estimated 7205 retinal ganglion cells dying yearly.⁴⁹⁻⁵¹ In our healthy controls, the decline in global MDB thickness with advancing age achieved borderline significance ($r = -0.256$; $p = 0.053$), which is similar to the age-related decline in global BMO-MRW noted by Chauhan *et al.* ($r = -0.26$; $p = 0.08$).²⁹ We also found a small but non-significant decline in RNFL thickness with age ($r = -0.135$; $p = 0.314$). The age disparity between the glaucoma and control groups likely enhanced the diagnostic performance of the parameters investigated. However, logistic regression analysis factoring for age showed that differences in AUROC values attributable to age did not reach statistical significance ($p = 0.262-0.999$) for any of the MDB or RNFL

parameters. Secondly, the study excluded subjects with pre-perimetric glaucoma, making the results generalizable only to glaucoma patients with existing VF defects. 12

Our segmentation program failed to correctly process the data of ten patients. Four patients had tilted retinas, and the change in the brightness of the RPE/BM complex across the image led to incomplete segmentation of this structure. For two patients, high noise produced numerous segmentation artifacts, and for four other patients, identification of the RPE/BM complex termination was incorrectly performed. In general, retinal blood vessels can make automated segmentation of neuroretinal rim structures difficult, since vessels located superficial to the RPE/BM complex absorb or scatter the light from the SD-OCT machine and cast shadows on the underlying RPE/BM layer.^{43,52-53} As this can lead to incomplete identification of the RPE/BM complex, the latest version of the 3D MDB algorithm incorporates a tool for minimizing interpolation errors. This modification has enabled the calculation of MDB thickness even in eyes in which large gaps in the RPE/BM complex contour are present due to vessel shadowing.

In conclusion, we found that MDB thickness from volume scans was excellent in differentiating eyes with glaucoma and early glaucoma from normal eyes. The diagnostic performance of MDB thickness for glaucoma was consistently equal or better than that of 2D RNFL thickness in all regions, particularly in the nasal quadrant and nasal sector subdivisions. The best combination of 3D MDB and 2D RNFL parameters for detecting glaucoma was also significantly better than all single 2D RNFL parameters alone. MDB thickness measurements using 3D volume scans may therefore be clinically useful in evaluating the neuroretinal rim in glaucoma.

Acknowledgements/Disclosures

13

A. Funding/Support: Teresa Chen, American Glaucoma Society Mid-Career Award (San Francisco, California), Massachusetts Lions Eye Research Fund, Fidelity Charitable Fund (Harvard University), Harvard Catalyst Grant (National Institutes of Health Award UL RR025758), Center for Biomedical OCT Research and Translation (National Institute of Biomedical Imaging and Bioengineering, National Institutes of Health Award P41 EB015903). **B. Financial Disclosures:** Vivek Srinivasan, Optovue, Inc (Fremont, California). Johannes de Boer, Dutch Technology Foundation, patents in Heidelberg Engineering (Heidelberg, Germany), past research support from NIDEK, Inc (Fremont, California), Terumo Corporation (Tokyo, Japan), Ninepoint Medical (Cambridge, Massachusetts). The other co-authors note no financial disclosures. **C. Other Acknowledgements:** design and conduct of the study (E.S., E.T., T.C.C), procurement of research funds (T.C.C.), collection (S.P., R.D., R.S.) and management of the data (E.S., R.L., C.Q., V.S., H.S., E.T.), data analysis (E.S., R.L., R.G., E.T.), and preparation (E.S., R.L.), review (R.G., R.S., E.T., T.C.C.), and approval of the manuscript (E.S., R.L., C.Q., V.S., R.G., R.D., S.P., H.S., R.S., E.T., J.D.B., T.C.).

References

14

1. Tielsch JM, Katz J, Quigley HA, Miller NR, Sommer A. Intraobserver and interobserver agreement in measurement of optic disc characteristics. *Ophthalmology*. 1988;95(3):350-356.
2. Wu H, de Boer JF, Chen TC. Reproducibility of retinal nerve fiber layer thickness measurements using spectral domain optical coherence tomography. *J Glaucoma*. 2011;20(8):470-476.
3. Kotowski J, Folio LS, Wollstein G, et al. Glaucoma discrimination of segmented cirrus spectral domain optical coherence tomography (SD-OCT) macular scans. *Br J Ophthalmol*. 2012;96(11):1420-1425.
4. Sung KR, Na JH, Lee Y. Glaucoma diagnostic capabilities of optic nerve head parameters as determined by Cirrus HD optical coherence tomography. *J Glaucoma*. 2012;21(7):498-504.
5. Wu H, de Boer JF, Chen TC. Diagnostic capability of spectral-domain optical coherence tomography for glaucoma. *Am J Ophthalmol*. 2012;153(5):815-826 e812.
6. Mwanza JC, Budenz DL, Godfrey DG, et al. Diagnostic performance of optical coherence tomography ganglion cell--inner plexiform layer thickness measurements in early glaucoma. *Ophthalmology*. 2014;121(4):849-854.
7. Mwanza JC, Oakley JD, Budenz DL, Anderson DR, Cirrus Optical Coherence Tomography Normative Database Study G. Ability of cirrus HD-OCT optic nerve head parameters to discriminate normal from glaucomatous eyes. *Ophthalmology*. 2011;118(2):241-248 e241.
8. Schulze A, Lamparter J, Pfeiffer N, Berisha F, Schmidtman I, Hoffmann EM. Diagnostic ability of retinal ganglion cell complex, retinal nerve fiber layer, and optic nerve head measurements by Fourier-domain optical coherence tomography. *Graefes Arch Clin Exp Ophthalmol*. 2011;249(7):1039-1045.
9. Na JH, Sung KR, Baek S, Sun JH, Lee Y. Macular and retinal nerve fiber layer thickness: which is more helpful in the diagnosis of glaucoma? *Invest Ophthalmol Vis Sci*. 2011;52(11):8094-8101.
10. Oddone F, Centofanti M, Tanga L, et al. Influence of disc size on optic nerve head versus retinal nerve fiber layer assessment for diagnosing glaucoma. *Ophthalmology*. 2011;118(7):1340-1347.
11. Sehi M, Grewal DS, Sheets CW, Greenfield DS. Diagnostic ability of Fourier-domain vs time-domain optical coherence tomography for glaucoma detection. *Am J Ophthalmol*. 2009;148(4):597-605.
12. Park SB, Sung KR, Kang SY, Kim KR, Kook MS. Comparison of glaucoma diagnostic Capabilities of Cirrus HD and Stratus optical coherence tomography. *Arch Ophthalmol*. 2009;127(12):1603-1609.
13. Moreno-Montanes J, Olmo N, Alvarez A, Garcia N, Zarranz-Ventura J. Cirrus high-definition optical coherence tomography compared with Stratus optical coherence tomography in glaucoma diagnosis. *Invest Ophthalmol Vis Sci*. 2010;51(1):335-343.

14. Asrani S, Essaid L, Alder BD, Santiago-Turla C. Artifacts in spectral-domain optical coherence tomography measurements in glaucoma. *JAMA Ophthalmol.* 2014;132(4):396-402. 15
15. Han IC, Jaffe GJ. Evaluation of artifacts associated with macular spectral-domain optical coherence tomography. *Ophthalmology.* 2010;117(6):1177-1189 e1174.
16. Liu Y, Simavli H, Que CJ, et al. Patient characteristics associated with artifacts in Spectralis optical coherence tomography imaging of the retinal nerve fiber layer in glaucoma. *Am J Ophthalmol.* 2015;159(3):565-576 e562.
17. Chong GT, Lee RK. Glaucoma versus red disease: imaging and glaucoma diagnosis. *Curr Opin Ophthalmol.* 2012;23(2):79-88.
18. Kim NR, Lim H, Kim JH, Rho SS, Seong GJ, Kim CY. Factors associated with false positives in retinal nerve fiber layer color codes from spectral-domain optical coherence tomography. *Ophthalmology.* 2011;118(9):1774-1781.
19. Leal-Fonseca M, Rebolleda G, Oblanca N, Moreno-Montanes J, Munoz-Negrete FJ. A comparison of false positives in retinal nerve fiber layer, optic nerve head and macular ganglion cell-inner plexiform layer from two spectral-domain optical coherence tomography devices. *Graefes Arch Clin Exp Ophthalmol.* 2014;252(2):321-330.
20. Povazay B, Hofer B, Hermann B, et al. Minimum distance mapping using three-dimensional optical coherence tomography for glaucoma diagnosis. *J Biomed Opt.* 2007;12(4):041204.
21. Chen TC. Spectral domain optical coherence tomography in glaucoma: qualitative and quantitative analysis of the optic nerve head and retinal nerve fiber layer (an AOS thesis). *Trans Am Ophthalmol Soc.* 2009;107:254-281.
22. Minckler DS, McLean IW, Tso MO. Distribution of axonal and glial elements in the rhesus optic nerve head studied by electron microscopy. *Am J Ophthalmol.* 1976;82(2):179-187.
23. Reis AS, O'Leary N, Yang H, et al. Influence of clinically invisible, but optical coherence tomography detected, optic disc margin anatomy on neuroretinal rim evaluation. *Invest Ophthalmol Vis Sci.* 2012;53(4):1852-1860.
24. Reis AS, Sharpe GP, Yang H, Nicoleta MT, Burgoyne CF, Chauhan BC. Optic disc margin anatomy in patients with glaucoma and normal controls with spectral domain optical coherence tomography. *Ophthalmology.* 2012;119(4):738-747.
25. Chauhan BC, Burgoyne CF. From clinical examination of the optic disc to clinical assessment of the optic nerve head: a paradigm change. *Am J Ophthalmol.* 2013;156(2):218-227 e212.
26. Pollet-Villard F, Chiquet C, Romanet JP, Noel C, Aptel F. Structure-function relationships with spectral-domain optical coherence tomography retinal nerve fiber layer and optic nerve head measurements. *Invest Ophthalmol Vis Sci.* 2014;55(5):2953-2962.
27. Strouthidis NG, Yang H, Reynaud JF, et al. Comparison of clinical and spectral domain optical coherence tomography optic disc margin anatomy. *Invest Ophthalmol Vis Sci.* 2009;50(10):4709-4718.
28. Strouthidis NG, Yang H, Fortune B, Downs JC, Burgoyne CF. Detection of optic nerve head neural canal opening within histomorphometric and spectral domain

- optical coherence tomography data sets. *Invest Ophthalmol Vis Sci.* 2009;50(1):214-223.
29. Chauhan BC, O'Leary N, Almobarak FA, et al. Enhanced detection of open-angle glaucoma with an anatomically accurate optical coherence tomography-derived neuroretinal rim parameter. *Ophthalmology.* 2013;120(3):535-543.
30. You JW, Chen TC, Mujat M, Park BH, de Boer JF. Pulsed illumination spectral-domain optical coherence tomography for human retinal imaging. *Opt Express.* 2006;14(15):6739-6748.
31. Maguluri G, Mujat M, Park BH, et al. Three dimensional tracking for volumetric spectral-domain optical coherence tomography. *Opt Express.* 2007;15(25):16808-16817.
32. Cense B, Nassif N, Chen T, et al. Ultrahigh-resolution high-speed retinal imaging using spectral-domain optical coherence tomography. *Opt Express.* 2004;12(11):2435-2447.
33. Heidelberg Engineering. Glaucoma Premium Edition. Anatomic Positioning System (APS). Heidelberg Engineering, Germany. Available at: <http://www.heidelbergengineering.com/>.
34. Gurses-Ozden R, Ishikawa H, Hoh ST, et al. Increasing sampling density improves reproducibility of optical coherence tomography measurements. *J Glaucoma.* 1999;8(4):238-241.
35. van der Schoot J, Vermeer KA, de Boer JF, Lemij HG. The effect of glaucoma on the optical attenuation coefficient of the retinal nerve fiber layer in spectral domain optical coherence tomography images. *Invest Ophthalmol Vis Sci.* 2012;53(4):2424-2430.
36. Drexler W, Fujimoto JG. State-of-the-art retinal optical coherence tomography. *Prog Retin Eye Res.* 2008;27(1):45-88.
37. Manjunath V, Shah H, Fujimoto JG, Duker JS. Analysis of peripapillary atrophy using spectral domain optical coherence tomography. *Ophthalmology.* 2011;118(3):531-536.
38. Staurenghi G, Sadda S, Chakravarthy U, Spaide RF, International Nomenclature for Optical Coherence Tomography P. Proposed lexicon for anatomic landmarks in normal posterior segment spectral-domain optical coherence tomography: the IN*OCT consensus. *Ophthalmology.* 2014;121(8):1572-1578.
39. Curcio CA, Saunders PL, Younger PW, Malek G. Peripapillary chorioretinal atrophy: Bruch's membrane changes and photoreceptor loss. *Ophthalmology.* 2000;107(2):334-343.
40. Jonas JB, Jonas SB, Jonas RA, et al. Parapapillary Atrophy: Histological Gamma Zone and Delta Zone. *PLoS ONE.* 2012;7(10):e47237.
41. El Chehab H, Delbarre M, Rosenberg R, Marill AF, Fenolland JR, Renard JP. New neuroretinal rim analysis with spectral domain optical coherence tomography, Spectralis (Heidelberg Engineering, Germany). Preliminary study. *J Fr Ophtalmol.* 2014;38(1):46-52.
42. Tun TA, Sun CH, Baskaran M, et al. Determinants of optical coherence tomography-derived minimum neuroretinal rim width in a normal chinese population. *Invest Ophthalmol Vis Sci.* 2015;56(5):3337-3344.

43. Almobarak FA, O'Leary N, Reis AS, et al. Automated segmentation of optic nerve head structures with optical coherence tomography. *Invest Ophthalmol Vis Sci.* 2014;55(2):1161-1168. 17
44. Danthurebandara VM, Sharpe GP, Hutchison DM, et al. Enhanced structure-function relationship in glaucoma with an anatomically and geometrically accurate neuroretinal rim measurement. *Invest Ophthalmol Vis Sci.* 2015;56(1):98-105.
45. Simavli H, Que CJ, Akduman M, et al. Diagnostic capability of peripapillary retinal thickness in glaucoma using 3D volume scans. *Am J Ophthalmol.* 2015;159(3):545-556 e542.
46. Badala F, Nouri-Mahdavi K, Raof DA, Leeprechanon N, Law SK, Caprioli J. Optic disk and nerve fiber layer imaging to detect glaucoma. *Am J Ophthalmol.* 2007;144(5):724-732.
47. Greaney MJ, Hoffman DC, Garway-Heath DF, Nakla M, Coleman AL, Caprioli J. Comparison of optic nerve imaging methods to distinguish normal eyes from those with glaucoma. *Invest Ophthalmol Vis Sci.* 2002;43(1):140-145.
48. lester M, Jonas JB, Mardin CY, Budde WM. Discriminant analysis models for early detection of glaucomatous optic disc changes. *Br J Ophthalmol.* 2000;84(5):464-468.
49. Balazsi AG, Rootman J, Drance SM, Schulzer M, Douglas GR. The effect of age on the nerve fiber population of the human optic nerve. *Am J Ophthalmol.* 1984;97(6):760-766.
50. Kerrigan-Baumrind LA, Quigley HA, Pease ME, Kerrigan DF, Mitchell RS. Number of ganglion cells in glaucoma eyes compared with threshold visual field tests in the same persons. *Invest Ophthalmol Vis Sci.* 2000;41(3):741-748.
51. Harwerth RS, Wheat JL, Rangaswamy NV. Age-related losses of retinal ganglion cells and axons. *Invest Ophthalmol Vis Sci.* 2008;49(10):4437-4443.
52. Lee K, Niemeijer M, Garvin MK, Kwon YH, Sonka M, Abramoff MD. Segmentation of the optic disc in 3-D OCT scans of the optic nerve head. *IEEE Trans Med Imaging.* 2010;29(1):159-168.
53. Golzan SM, Avolio A, Graham SL. Minimising retinal vessel artefacts in optical coherence tomography images. *Comput Methods Programs Biomed.* 2011;104(2):206-211.

Legend

18

Figure 1: Automated segmentation of 3D volume scans and determination of minimum distance band (MDB) thickness in the right eye of a 78-year-old healthy female subject (top row) and the left eye of a 64-year-old female subject with - pigmentary glaucoma (bottom row). *Left column:* B-scan images of the midsection of the optic nerve head. The OCT-derived optic disc rim, defined as the termination of the retinal pigment epithelium/Bruch's membrane complex (RPE/BM complex; red dots), and the internal limiting membrane (ILM; green dots) were automatically segmented using an internally-developed algorithm. *Middle column:* Infrared reflectance images of the optic nerve head. The RPE/BM complex termination, represented by 100 points spaced by 3.6 degrees (red dots), was superimposed on the image to verify the accuracy of the disc rim. *Right column:* The neuroretinal rim reconstructed in three-dimensions. Minimum distance band (MDB; solid blue) thickness was calculated as the distance between points along the RPE/BM complex termination (red dots) and the closest corresponding points on the ILM (blue dots).

Table 1: Characteristics of the study population of normal, glaucoma, and early glaucoma patients

	Normal	Glaucoma	p*	Early glaucoma	p**
Number of eyes	58	105		31	
Number of right eyes/left eyes	32/26	53/52	0.566	21/10	0.250
Mean age (years)	54.3 ± 15.5	68.0 ± 11.9	<.0001	68.9 ± 9.8	<.0001
Gender (% female)	69.0	45.7	0.004	45.2	0.029
Race (%)			0.152		0.107
African American	13.8	21.0		12.9	
Asian	8.6	3.8		9.7	
Caucasian	65.5	65.7		71.0	
Hispanic	12.1	5.7		0	
Other	0	3.8		6.5	
Refractive error (D)					
Spherical equivalent	-0.07 ± 1.73	-0.23 ± 1.71	0.572	-0.02 ± 1.73	0.899
Visual field					
Mean deviation (dB)	-1.42 ± 1.93	-11.89 ± 7.58	<.0001	-3.72 ± 1.45	<.0001
Pattern standard deviation (dB)	1.52 ± 0.29	8.35 ± 3.20	<.0001	4.96 ± 1.74	<.0001

D=diopiter; dB=decibel

Results are expressed as the mean ± standard deviation unless otherwise indicated

*normal vs. glaucoma

**normal vs. early glaucoma

Table 2: Neuroretinal rim thickness measurements derived from optical coherence tomography volume scans of normal, glaucoma, and early glaucoma patients

Neuroretinal rim minimum distance band (MDB) location	Normal Mean \pm SD (μm)	Glaucoma* Mean \pm SD (μm)	Early glaucoma* Mean \pm SD (μm)
Global	307.5 \pm 41.2	171.0 \pm 51.5	203.6 \pm 44.3
Inferior	341.6 \pm 52.0	167.5 \pm 62.0	195.3 \pm 62.5
Superior	337.7 \pm 53.8	178.6 \pm 66.2	222.1 \pm 61.2
Nasal	312.4 \pm 49.5	189.7 \pm 67.9	228.7 \pm 63.0
Temporal	239.4 \pm 45.1	148.6 \pm 50.0	168.4 \pm 46.4
IN	359.6 \pm 57.4	191.9 \pm 71.1	226.3 \pm 64.7
SN	349.0 \pm 59.2	192.7 \pm 73.3	231.2 \pm 69.8
IT	323.5 \pm 56.3	142.9 \pm 63.3	163.6 \pm 71.9
ST	335.8 \pm 51.5	169.7 \pm 69.6	214.1 \pm 65.1

SD: standard deviation; μm : micrometers; IN: inferior-nasal sector; SN: superior-nasal sector; IT: inferior-temporal sector; ST: superior-temporal sector
 * $p < 0.0001$ for all when compared to normal patients

Table 3: Diagnostic capabilities of three-dimensional (3D) versus two-dimensional (2D) optical coherence tomography parameters for glaucoma: 3D minimum distance band (MDB) parameter versus 2D retinal nerve fiber layer (RNFL) thickness parameter

Location of optical coherence tomography parameter	Glaucoma group [AUROC (SE)]	p*	Early glaucoma group [AUROC (SE)]	p**	p***
MDB thickness from volume scans					
Global	0.969 (0.0122)	0.313	0.952 (0.0209)	0.377	
Inferior	0.966 (0.0146)	0.529	0.949 (0.0248)	0.515	
Superior	0.962 (0.0131)	0.144	0.924 (0.0285)	0.270	
Nasal	0.916 (0.0214)	0.023	0.848 (0.0417)	0.084	
Temporal	0.907 (0.0258)	0.177	0.870 (0.0427)	0.084	
IN	0.951 (0.0179)	0.049	0.923 (0.0297)	0.084	
SN	0.942 (0.0176)	0.023	0.900 (0.0336)	0.111	
IT	0.966 (0.0141)	0.529	0.944 (0.0287)	0.536	
ST	0.964 (0.0126)	0.089	0.932 (0.0264)	0.084	
RNFL thickness					
Global	0.954 (0.0156)		0.928 (0.0262)		
Inferior	0.958 (0.0142)		0.929 (0.0299)		
Superior	0.936 (0.0181)		0.882 (0.0364)		
Nasal	0.820 (0.0329)		0.711 (0.0607)		
Temporal	0.858 (0.0294)		0.756 (0.0593)		
IN	0.898 (0.0232)		0.824 (0.0460)		
SN	0.869 (0.0271)		0.815 (0.0477)		
IT	0.958 (0.0150)		0.924 (0.0345)		
ST	0.932 (0.0207)		0.868 (0.0388)		
Best combinations					
Inferior MDB, ST MDB, SN MDB, and inferior RNFL	0.984 (0.0091)				
Inferior MDB, ST MDB, and SN MDB	0.981 (0.0093)				0.319
Inferior RNFL and ST RNFL	0.966 (0.0138)				0.018

SE: standard error

IN: inferior-nasal sector; SN: superior-nasal sector; IT: inferior-temporal sector; ST: superior-temporal sector

*MDB AUROC value vs. AUROC value of corresponding RNFL thickness measurement in glaucoma

**MDB AUROC value vs. AUROC value of corresponding RNFL thickness measurement in early glaucoma

***MDB AUROC value vs. AUROC value of the and-logic combination of inferior MDB, ST MDB, SN MDB, and inferior RNFL

Table 4: Diagnostic performance of the optical coherence tomography minimum distance band (MDB) parameter in glaucoma: best sensitivities and specificities

Neuro-retinal rim (MDB) location	Sensitivity (CI)	Specificity (CI)	PPV (CI)	NPV (CI)	Sensitivity at fixed 95% specificity
Global	89.5 (83.7-95.4)	96.6 (91.9-100.0)	98.0 (95.1-100.0)	83.6 (74.7-92.5)	89.5 (71.5-96.7)
Inferior	92.4 (87.3-97.5)	96.6 (91.9-100.0)	98.0 (95.2-100.0)	87.5 (79.4-95.6)	92.4 (76.4-97.8)
Superior	91.4 (86.1-96.8)	89.7 (81.8-97.5)	94.1 (89.6-98.7)	85.3 (76.4-94.2)	76.2 (53.3-90.0)
Nasal	78.1 (70.2-86.0)	93.1 (86.6-99.6)	95.4 (90.9-99.8)	70.1 (59.9-80.4)	71.4 (48.0-87.2)
Temporal	86.7 (80.2-93.2)	89.7 (81.8-97.5)	93.8 (89.0-98.6)	78.8 (68.9-88.7)	65.7 (42.0-83.5)
IN	89.5 (83.7-95.4)	93.1 (86.6-99.6)	95.9 (92.0-99.8)	83.1 (74.0-92.2)	83.8 (63.0-94.0)
SN	88.6 (82.5-94.7)	91.4 (84.2-98.6)	94.9 (90.5-99.3)	81.5 (72.1-91.0)	71.4 (47.9-87.2)
IT	91.4 (86.1-96.8)	96.6 (91.9-100.0)	98.0 (95.2-100.0)	86.2 (77.8-94.6)	91.4 (74.7-97.5)
ST	87.6 (81.3-93.9)	93.1 (86.6-99.6)	95.8 (91.8-99.8)	80.6 (71.1-90.1)	79.0 (56.8-91.6)

CI: 95% confidence interval; PPV: positive predictive value; NPV: negative predictive value; IN: inferior-nasal sector; SN: superior-nasal sector; IT: inferior-temporal sector; ST: superior-temporal sector

Table 5: Diagnostic performance of the optical coherence tomography minimum distance band (MDB) parameter in early glaucoma: best sensitivities and specificities

MDB location	Sensitivity (CI)	Specificity (CI)	PPV (CI)	NPV (CI)	Sensitivity at fixed 95% specificity
Global	96.8 (90.6-100.0)	84.5 (75.2-93.8)	76.9 (63.7-90.2)	98.0 (94.1-100.0)	77.4 (49.4-92.3)
Inferior	87.1 (75.3-98.9)	96.6 (91.9-100.0)	93.1 (83.9-100.0)	93.3 (87.0-99.7)	87.1 (61.0-96.7)
Superior	93.6 (84.9-100.0)	82.8 (73.0-92.5)	74.4 (60.7-88.1)	96.0 (90.6-100.0)	48.4 (23.5-74.1)
Nasal	67.7 (51.3-84.2)	87.9 (79.6-96.3)	75.0 (59.0-91.0)	83.6 (74.3-92.9)	41.9 (19.0-69.0)
Temporal	80.7 (66.7-94.6)	89.7 (81.8-97.5)	80.7 (66.7-94.6)	89.7 (81.8-97.5)	45.2 (21.2-71.6)
IN	80.7 (66.7-94.6)	93.1 (86.6-99.6)	86.2 (73.7-98.8)	90.0 (82.4-97.6)	74.2 (45.9-90.7)
SN	80.7 (66.7-94.6)	91.4 (84.2-98.6)	83.3 (70.0-96.7)	89.8 (82.1-97.5)	48.4 (23.5-74.1)
IT	83.9 (70.9-96.8)	96.6 (91.9-100.0)	92.9 (83.3-100.0)	91.8 (84.9-98.7)	83.9 (56.9-95.4)
ST	96.8 (90.6-100.0)	81.0 (71.0-91.1)	73.2 (59.6-86.7)	97.9 (93.9-100.0)	58.0 (31.0-81.0)

CI: 95% confidence interval; PPV: positive predictive value; NPV: negative predictive value; IN: inferior-nasal sector; SN: superior-nasal sector; IT: inferior-temporal sector; ST: superior-temporal sector

Table 6: Diagnostic performance of optical coherence tomography retinal nerve fiber layer (RNFL) thickness in glaucoma: best sensitivities and specificities

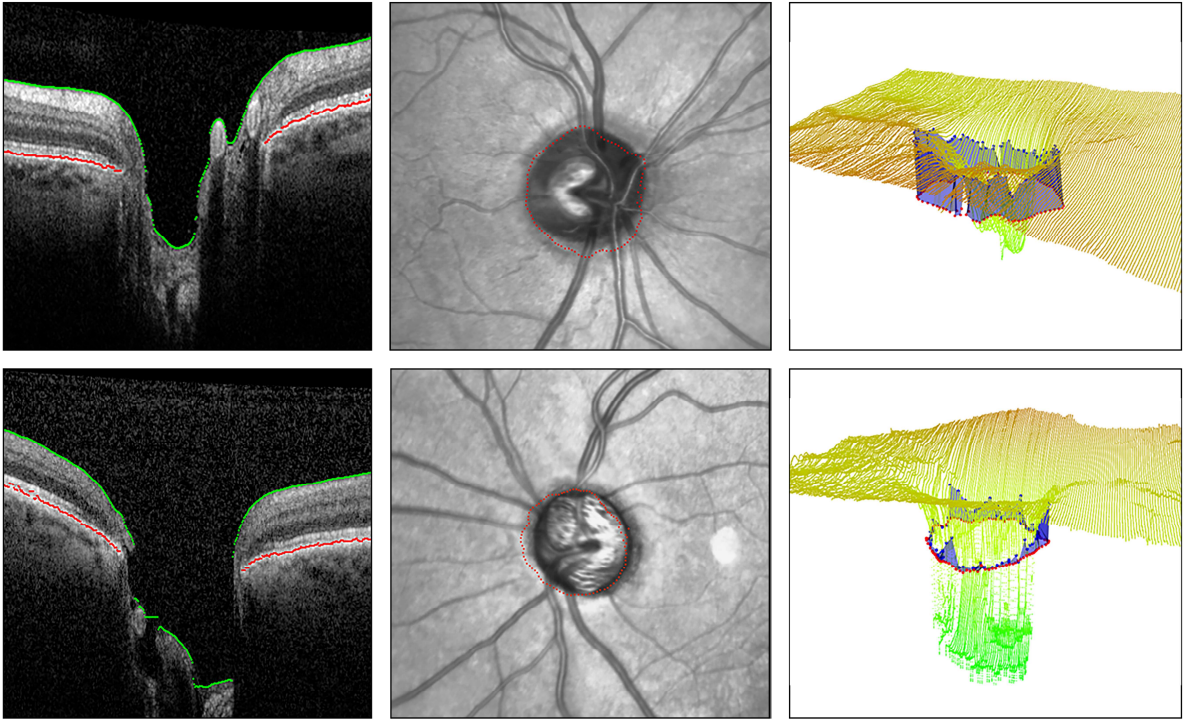
RNFL location	Sensitivity (CI)	Specificity (CI)	PPV (CI)	NPV (CI)	Sensitivity at fixed 95% specificity
Global	86.7 (80.2-93.2)	93.1 (86.6-99.6)	95.8 (91.8-99.8)	79.4 (69.8-89.0)	83.8 (63.0-94.0)
Inferior	88.6 (82.5-94.7)	96.6 (91.9-100.0)	97.9 (95.0-100.0)	82.4 (73.3-91.4)	89.5 (71.5-96.7)
Superior	81.0 (73.4-88.5)	94.8 (89.1-100.0)	96.6 (92.8-100.0)	73.3 (63.3-83.3)	78.1 (55.6-91.0)
Nasal	83.8 (76.8-90.9)	69.0 (57.0-80.9)	83.0 (75.9-90.2)	70.2 (58.3-82.1)	51.4 (29.1-73.2)
Temporal	78.1 (70.2-86.0)	87.9 (79.6-96.3)	92.1 (86.5-97.7)	68.9 (58.4-79.5)	57.1 (33.9-77.6)
IN	72.4 (63.8-80.9)	91.4 (84.2-98.6)	93.8 (88.6-99.1)	64.6 (54.3-75.0)	62.9 (39.2-81.6)
SN	71.4 (62.8-80.1)	86.2 (77.3-95.1)	90.4 (8.4-96.7)	62.5 (51.9-73.1)	59.0 (35.6-79.0)
IT	92.4 (87.3-97.5)	93.1 (86.6-99.6)	96.0 (92.2-99.8)	87.1 (78.8-95.4)	83.8 (63.0-94.0)
ST	88.6 (82.5-94.7)	86.2 (77.3-95.1)	92.1 (86.8-97.4)	80.7 (70.8-90.5)	69.5 (45.9-86.0)

CI: 95% confidence interval; PPV: positive predictive value; NPV: negative predictive value; IN: inferior-nasal sector; SN: superior-nasal sector; IT: inferior-temporal sector; ST: superior-temporal sector

Table 7: Diagnostic performance of optical coherence tomography retinal nerve fiber layer (RNFL) thickness in early glaucoma: best sensitivities and specificities

RNFL location	Sensitivity (CI)	Specificity (CI)	PPV (CI)	NPV (CI)	Sensitivity at fixed 95% specificity
Global	90.3 (79.9-100.0)	81.0 (71.0-91.1)	71.8 (57.7-85.9)	94.0 (87.4-100.0)	67.7 (39.5-87.1)
Inferior	83.9 (70.9-96.8)	93.1 (86.6-99.6)	86.7 (74.5-98.8)	91.5 (84.4-98.6)	80.6 (53.0-93.9)
Superior	77.4 (62.7-92.1)	84.5 (75.2-93.8)	72.7 (57.5-87.9)	87.5 (78.8-96.2)	58.1 (31.0-81.0)
Nasal	77.4 (62.7-92.1)	69.0 (57.1-80.9)	57.1 (42.2-72.1)	85.1 (74.9-95.3)	22.5 (7.7-50.6)
Temporal	64.5 (47.7-81.4)	87.9 (79.6-96.3)	74.1 (57.5-90.6)	82.3 (72.8-91.8)	41.9 (19.0-69.0)
IN	87.1 (75.3-98.9)	69.0 (57.1-80.9)	60.0 (45.7-74.3)	90.9 (82.4-99.4)	29.0 (11.1-57.4)
SN	90.3 (79.9-100.0)	58.6 (46.0-71.3)	53.9 (40.3-67.4)	91.9 (83.1-100.0)	45.2 (21.2-71.6)
IT	87.1 (75.3-98.9)	93.1 (86.6-99.6)	87.1 (75.3-98.9)	93.1 (86.6-99.6)	71.0 (42.6-88.9)
ST	87.1 (75.3-98.9)	74.1 (62.9-85.4)	64.3 (49.8-78.8)	91.5 (83.5-99.5)	38.7 (16.8-66.3)

CI: 95% confidence interval; PPV: positive predictive value; NPV: negative predictive value; IN: inferior-nasal sector; SN: superior-nasal sector; IT: inferior-temporal sector; ST: superior-temporal sector



ACCEPTED MANUSCRIPT